Microchimica Acta (2018) 185: 74
https://doi.org/10.1007/s00604-017-2611-7

ORIGINAL PAPER

Nanodiamonds conjugated to gold nanoparticles for colorimetric detection of clenbuterol and chromium(III) in urine

Muthaiah Shellaiah[1] · Turibius Simon[2] · Parthiban Venkatesan[1] · Kien Wen Sun[1,3] · Fu-Hsiang Ko[2] · Shu-Pao Wu[1]

Received: 18 July 2017 / Accepted: 6 December 2017 / Published online: 20 December 2017
© Springer-Verlag GmbH Austria, part of Springer Nature 2017

Abstract

Nanodiamonds were modified such that they carry thiol groups (**ND-thiol**). Gold nanoparticles were reacted with **ND-thiol** to obtain a highly stable conjugate of the type **ND**@AuNPs. Both **ND-thiol** and the **ND**@AuNPs were characterized by SEM, TEM, AFM, DLS, zeta potential, XPS, XRD, UV-Vis, Raman, FTIR and cytotoxicity studies. Their biocompatibility was confirmed via an MTT assay with HeLa cells. At a pH value of 6, the **ND**@AuNPs represent a colorimetric probe that can be used to selectively detect the illegally used β-adrenergic drug clenbuterol (CLB) and the pollutant chromium(III). Detection can be performed visually by monitoring the color change from wine red to purple blue, or by colorimetric measurement of the so-called SPR peaks at 651 and 710 nm. The color changes are due to aggregation, and this is confirmed by TEM and DLS data. The involvement of surface functional groups that assist in analyte recognition was verified by FTIR. The detection limits are 0.49 nM for CLB, and 0.37 nM for Cr(III). The **ND**@AuNPs were successfully applied to the determination of Cr(III) and CLB in spiked human urine samples. Notably, the low interference by other ions in the detection of Cr(III) in tap and lake water is confirmed by ICP-MS analyses.

Keywords Gold nanoparticles · Nanocomposite · β-Adrenergic drug assay · Chromium(III) recognition · pH effective sensor · Surface plasmon resonance · Sub-nanomolar detection · Urine analysis · Water analysis

Introduction

Clenbuterol hydrochloride [CLB] is a well-known drug moiety utilized in the treatment of asthma as bronchodilator and in human and veterinary heart tonics. Further to notice, CLB possess the pharmacological similarities to epinephrine and salbutamol [1]. However, still, it has been illegally used as a stimulating drug for the production of lean meat. The presence of high CLB residues in those livestock can lead to serious side effects and food poisoning [2]. Therefore, several methods were reported for CLB detection, including gas chromatography with mass spectrometry [3], enzyme-linked immunosorbent assay [4], liquid chromatography with mass spectrometry [5], capillary electrophoresis with amperometric [6], surface plasmon resonance and electrochemical impedance spectroscopy [7]. But, due to the requirement of high cost instruments, time consumption as well as the difficulty in sample preparation, the highly precise, reliable, and low-cost methods are still in need. Wherein, those requirements were fulfilled by the gold nanoparticles (AuNPs) based colorimetric assay of CLB [8].

In a similar manner, Cr(III) ions are known as contaminant in vitro and can act as a competitive inhibitor of several cellular processes [9]. Moreover, it plays the potential role in sustaining proper carbohydrate and lipid metabolism at a molecular level [10]. But, in excess, it may cause genotoxic effects and its deficit resulting in sugar metabolic disorder led to the engendering diabetes, even cataract, cardiovascular disorders, blindness and uremia [11]. Hence, numerous approaches have been described for Cr(III) detection, comprising

Electronic supplementary material The online version of this article (https://doi.org/10.1007/s00604-017-2611-7) contains supplementary material, which is available to authorized users.

✉ Kien Wen Sun
kwsun@mail.nctu.edu.tw

[1] Department of Applied Chemistry, National Chiao Tung University, Hsinchu 300, Taiwan

[2] Department of Materials Science and Engineering, National Chiao Tung University, Hsinchu 300, Taiwan

[3] Department of Electronics Engineering, National Chiao Tung University, Hsinchu 300, Taiwan

inductively coupled plasma-mass spectroscopy or inductively coupled atomic absorption/emission spectroscopy, electrothermal atomic absorption spectrometry, electrolysis and voltammetry, potentiometric membrane sensoring, fluorescence imaging, chemiluminescence [12–17]. However, many of them display low selectivity, low sensitivity, needing expensive instruments, and delayed responses. Which allows many researchers to develop AuNPs based probes for high sensitive and simplistic colorimetric naked eye detection of Cr(III) ions [18].

On the other hand, nanocomposites based detection of CLB and Cr(III) ions also seems to be promising [19, 20]. Towards this approach, with respect to biological utilities, AuNPs attached nanodiamonds (NDs) can be considered as a suitable candidate [21]. Wherein, NDs may act as a stabilizer by mediating between the AuNPs to prevent the aggregation. Which can be further stimulated via modification of NDs such that they carry amide ligands and thiol groups as reported recently [22].

In this report, nanodiamonds were modified via functionalization of 4-aminothiophenol to afford **ND-Thiol**. Which was further reacted with AuNPs to obtain a highly stable conjugate of the type **ND**@AuNPs. Both **ND-thiol** and **ND**@AuNPs were characterized by SEM, TEM, AFM, DLS, zeta potential, XPS, XRD, UV-Vis, Raman, FTIR and cytotoxicity studies. At pH 6, the **ND**@AuNPs act as a colorimetric probe for the selective detection of CLB and Cr(III) ions in real water and urine sample.

Experimental

The general information on metal ions, Instruments used, sample preparation procedures for SEM, TEM, FTIR studies, synthetic procedures, characterization, optimization details and MTT assay protocols of **ND-Thiol** and **ND**@AuNPs with respective data are provided in Electronic Supporting Material (ESM).

Conjugation of bare AuNPs with ND-thiol

The bare AuNPs were synthesized via borohydride reduction method as reported previously [18]. To the 20 mL of synthesized bare AuNPs, 200 μL of **ND-Thiol** was added from **ND-Thiol** dispersion (1 $\mu g.mL^{-1}$), which maintained the final concentration of **ND-Thiol** in **ND**@AuNPs as 10 $ng.mL^{-1}$. The colloidal solution was stirred in the dark for 30 min at room temperature. The wine-red aqueous solution of **ND**@AuNPs were stored at room temperature and evidenced the stability for at least four months. The average size of the **ND**@ AuNPs were determined by DLS and TEM micrographic studies. Those **ND**@AuNPs were directly utilized in colorimetric assay titrations. For XRD data, it has been centrifuged at 14000 rpm and under vaccum to obtain the powder, which states that 25 mg of **ND**@AuNPs were present in 100 ml solution.

Colorimetric assay protocol

To a 790 μL of solution containing **ND**@AuNPs, 200 μL of pH 6 buffer, 10 μL of either CLB (1 μM) or other interferences (3 μM) were added separately. However, the final volume of the above mixture was maintained as 1 mL. The mixture was sustained at room temperature for 25 min and then transferred separately into a 1.0 cm quartz cell. The absorption spectra were recorded by UV-Vis spectrometer between 450 to 800 nm wavelength ranges. Subsequently, the above procedure has been employed for the detection of Cr(III) at 1 μM and other metal ions at 3 μM or Cr(VI) at 5 μM. Similarly, for dual analyte investigations, the concentration of CLB or Cr(III) ions were kept at 1 μM along with other interferences at 3 μM or Cr(VI) at 5 μM [for Cr(III)].

For individual titrations, to a 790 μL of **ND**@AuNPs solution, 200 μL of pH 6 buffer, 10 μL of different concentrations of CLB or Cr(III) (0–1000 nM) were added separately. The final volume of the mentioned mixture kept as 1 mL at room temperature for 25 min and then transferred separately into a 1.0 cm quartz cell. The absorption spectra were recorded by UV-Vis spectrometer.

Analysis of CLB or Cr^{3+} in real samples

Water samples of our laboratory tap and lake located in NCTU, Hsinchu, Taiwan, were collected and filtered through a 0.2 μm membrane. To the 200 μL of lake or tap water, different volumes (0.4, 1, and 4 μL) of Cr^{3+} ions standard solution (10 and 100 μM) were spiked, individually. Those samples were then added to the solution containing 700 μL of **ND**@AuNPs and 100 μL pH 6 buffer, preserved at room temperature for 25 min. The final concentrations of Cr^{3+} ions were maintained as 0.01, 0.25, and 1.0 μM, respectively. Thereafter, the analytical results were found by ICP-MS and from the established sensing method. Above mentioned procedure was applied for DI water and urine based assay of CLB or Cr^{3+} ions.

Results and discussion

Synthesis and properties of ND-thiol

As shown in Scheme S1 (ESM), the **ND-Thiol** was synthesized based on our previous report [22]. Those **ND-Thiol**

particles were characterized through FTIR, Raman, XPS, zeta potential, SEM, TEM and AFM studies as detailed in ESM with respective data (Figs. S1-S10). Impressively, as shown in Fig. 1a, b, the surface modified ND derivative visualize the diverse particle sizes and morphologies as further described in ESM (See characterization of **ND-Thiol**).

Optimization of method

The following parameters were optimized (a) **ND-Thiol** concentration in **ND**@AuNPs (b) sample pH value in assay; (c) reaction time. Respective data and Figures are given in the ESM (Figs. S11, S22~S24). The following experimental conditions were found to give best results: (a) 10 ng.mL^{-1} of **ND-Thiol** in **ND**@AuNPs (b) A sample pH value of 6; (c) 25 min reaction time.

Characterization of ND@AuNPs

As shown in Scheme S2 (ESM) bare AuNPs were modified by the addition of **ND-Thiol** (10 ng.mL^{-1}). Hence, those NPs are represented as **ND**@AuNPs. During the above modification, the SPR peak of bare AuNPs (520 nm) seems to be red shifted to 523 nm with the stability over a period of four months (Figs. S12a and b, ESM). Additionally, HR-TEM of **ND**@AuNPs clarify the conjugation between **ND-Thiol** and AuNPs as exposed in Fig. 1c, d. The diffraction of 0.207 and 0.241 nm are corresponds to (111) pattern of nanodiamond and Au [23, 24], respectively. Similarly, the FT pattern of selected AuNP (Fig. S13, ESM), notify the (111) and (200) patterns. Next, from Figs. S14a and b (ESM), the XRD peaks (2) of AuNPs at 38.03°, 44.18°, 64.45°, 77.42°, 82.15° and 98.23° can be associated to (111), (200), (220), (311), (222) and (400) crystalline planes of Au atom, respectively, and from JCPDS file (JCPDS no. 01–1174), it can be assigned as face-centered cubic (fcc) phase [25]. Further, the presence of **ND-Thiol** can be established from its low intense XRD peaks at 44.69° and 75.13° related to (111) and (220) patterns of diamond [26].

In a similar fashion, as shown in Fig. S14c (ESM), the XPS data [27] at 88.5 and 84.9 eV are apportioned to original 4f spectrum of Au atom [87.8 eV (Au $4f_{5/2}$) and 84.2 eV (Au $4f_{7/2}$)]. The distorted XPS values may attributed to the

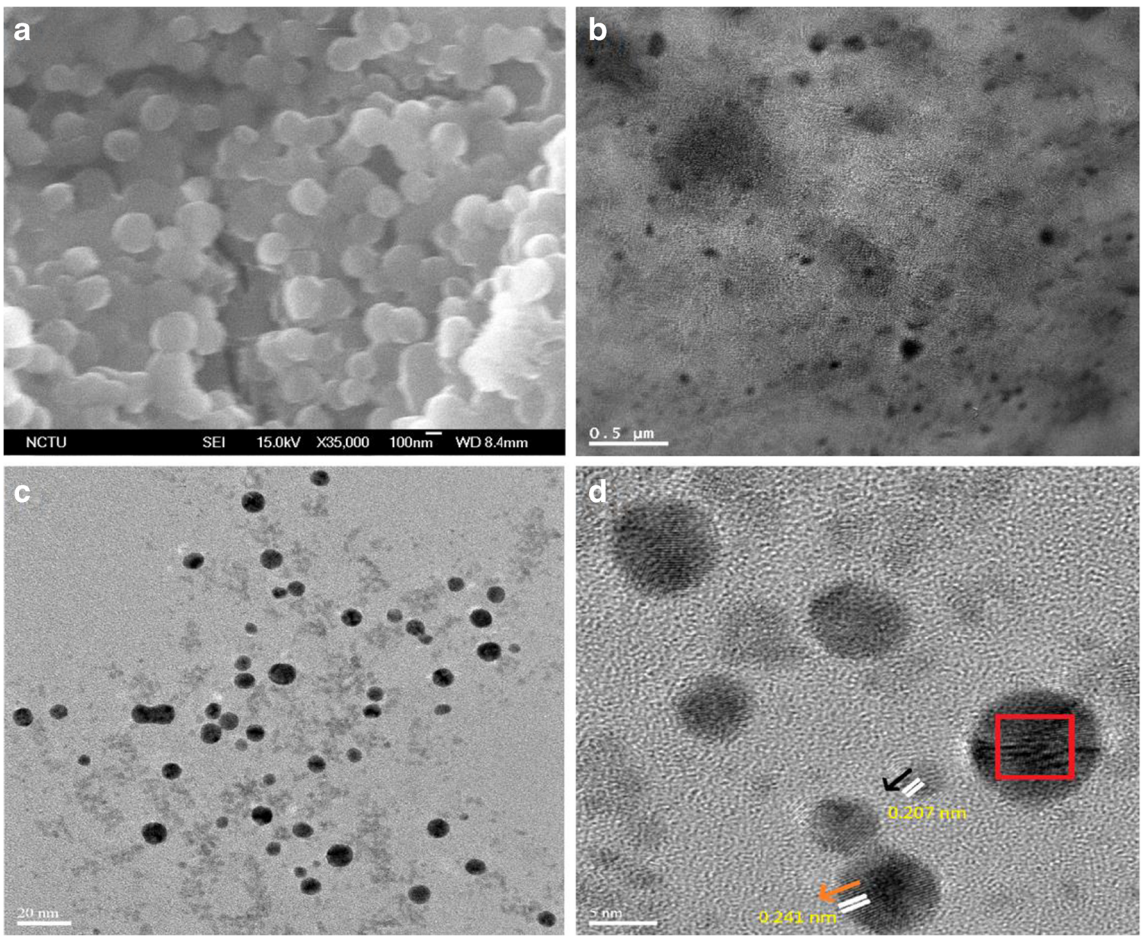

Fig. 1 **a, b** SEM and TEM and AFM images of **ND-Thiol** nanoparticles (at 1 μg. mL^{-1} in water dispersion); **c** TEM of **ND**@AuNPs (**ND-Thiol** = 10 ng.mL^{-1}); **d** High magnified TEM image of **ND**@AuNPs; 0.207 and 0.241 nm diffraction representing (111) pattern of diamond and AuNPs, respectively

presence of **ND-Thiol** over AuNPs surface. Interestingly, co-existence of **ND-Thiol** has also been countersigned by its XPS peak at 284.8 eV (Fig. S14d, ESM). Next, particle size of bare AuNPs (5.2 ± 3.7 nm) has been affected during the modification by **ND-Thiol** and increased to 19.3 ± 11.8 nm (Figs. S15 and S16, ESM). Moreover, **ND**@AuNPs displayed the slightly affected zeta potential (−27.80 mV) than that of bare AuNPs (−31.33 mV), as shown in Figs. S17 and S18 (ESM). Hence, stabilization through the repulsive -Ve charges is represented in Fig. S19 (ESM).

MTT assay of ND-thiol and ND@AuNPs

Initially, the cytotoxicity of **ND-Thiol** was evaluated from four parallel experiments. In which, similar to previous reports, all the nanodiamond derivatives displays their low toxicities in Hela cells (Fig. S20, ESM). Further, **ND-Thiol** witnessed the more than 85% of cell viability even at 100 $\mu g.mL^{-1}$, which confirms its biocompatibility and allows us to capitalize in the stabilization of AuNPs. Next, cytotoxicity studies on **ND**@AuNPs in HeLa cells (four parallel measurements) revealed its negligible toxicity even at 150 $\mu g.mL^{-1}$ concentration as publicised in Figs. S21a (ESM). Wherein, **ND**@AuNPs indicates the 84% cell viability. Furthermore, by plotting **ND**@AuNPs concentration Vs cell viability, the 50% cell survival concentration value (IC_{50}) is predicted to be 237 $\mu g.mL^{-1}$ as seen in Fig. S21b (ESM). Hence, confirmed its intracellular permeability and low cytotoxicity to apply in environmental and biological samples based analyte detection.

Selective CLB and Cr(III) assay by ND@AuNPs

As depicted in Fig. 2a, b, contrast to other interferences [NaCl, $CaCl_2$, Thr (Threonine), Glu (Glutamic Acid), Urea, Tyr (Tyrosine), Glucose, Orn (Ornithine), His (Histidine), AA (Ascorbic Acid), Ala (Alanine), Sal (Salbutamol), Leu (Leucine), Rct (Ractopamine), Cys (Cysteine), HCys (Homo Cysteine), Gly (Glycine) and Lys (Lysine) fixed at 3 μM], the clenbuterol (CLB) at 1 μM is incredibly affected the SPR peak of **ND**@AuNPs with wine red to purple colorimetric variation. At this point, the initial SPR peak (at 523 nm) is reduced and red shifted to 531 nm with gradual appearance of newer band at 651 nm. In the same way, Cr(III)ions (at 1 μM) are evidenced the better selectivity than that of other metal ions [Na(I), Ni(II), Fe(III), Cd(II), Ca(II), Ga(III), Cu(II), Fe(II), Mg(II), Ba(II), Al(III), Ag(I), Co(II), Zn(II), Pb(II), Mn(II), In(III), and Hg(II)] at 3 μM and Cr(VI) at 5 μM via SPR and colorimetric responses as shown in Fig. 2c, d. But, Cr(III) induce the purple blue color with quenched-red shifted SPR peak at 533 nm along with the formation of inferior band at 710 nm.

Very impressively, the **ND**@AuNPs based diverse assay of CLB and Cr(III) has been demonstrated by the newer SPR peaks at 651 and 710 nm, respectively. Subsequently, the single and dual analyte studies (Figs. S25a and b, ESM) are well supported its better selectivity towards CLB and Cr(III) ions via SPR ratio bar graphs at A_{651}/A_{523} and A_{710}/A_{523}, congruently. In which, CLB detection is slightly affected only in presence of Ractopamine. Whereas, the other β-adrenergic drug Salbutamol have negligible effect. On the other hand, during single analyte studies, the Cr(VI) ions at 5 μM evidenced mild aggregation induced color change. But, in dual analyte investigation not shown any interference. This confirmed the enhanced selectivity of Cr(III) ions than that of all metal ions. Further to protract the utility of **ND**@AuNPs based assay, the time effect with respect to concentration between 0 and 1 μM (with an equal span of 0.2 μM) of CLB and Cr(III)ions has been taken into account. Wherein, both of them envisioned the immediate color alteration (wine red to purple blue) from 0.4 μM onwards as presented in Figs. S26 and S27 (ESM). Those responses are further enhanced after 10 and 20 min of time intervals. Excitingly, contrary other strategy based detections [28, 29], the **ND**@AuNPs detect the CLB at 0.15 μM via visualization of purple blue color after 25 min.

Detection mechanism and limits

As seen in Fig. 4a, b, upon addition of 0–1 μM of CLB, or Cr(III) ions to aqueous **ND**@AuNPs (at pH 6), gradual incremental peaks are observed at 651 or 710 nm, respectively. At the same time, the origin SPR peak at 523 nm is red shifted to 531 or 533 nm, correspondingly. Moreover, due to the aggregation induced by CLB and Cr(III) ions, the wine red color is changed in to purple blue. Which is approved by the TEM images as displayed in Figs S28a and b (ESM). Consistently, the DLS study revealed the 2.2 and 2.8 times enhanced particle sizes of **ND**@AuNPs with CLB and Cr(III) and predicted as 73.5 ± 26.5 and 96.2 ± 68 nm (Figs. S28c and d, ESM), individually.

Next, the exact binding forces and functional group involvement, FTIR studies [30] are described as follows. Firstly, as exposed in Fig. S29 (ESM), contrast to **ND-Thiol**, a broad amide –NH band is lies between 2900~3500 cm^{-1} for **ND**@AuNPs. Similarly, the symmetrical amide –NH stretch is discovered an upshifted band at 1412 cm^{-1}. Further to note, the –C-N stretching bands of **ND**@AuNPs are found at 1195 and 2263 cm^{-1}. Moreover, the disappearance of free –SH (at 2577 cm^{-1}) band along with presence of downshifted amide –C=O band at 1655 cm^{-1} is proved the **ND-Thiol** conjugation over AuNPs. During coordination with CLB, the –C-N stretching bands are downshifted to 1225 and 2400 cm^{-1} as publicized in Fig. S30 (ESM). Interestingly, due to the H-bonded coordination with –NH_2, -NH and OH of clenbuterol, the amide –C=O band is upshifted to 1599 cm^{-1}. Similarly, the involvement of amide –NH group in H-bonding formation with 'chlorine (Cl)' of CLB is

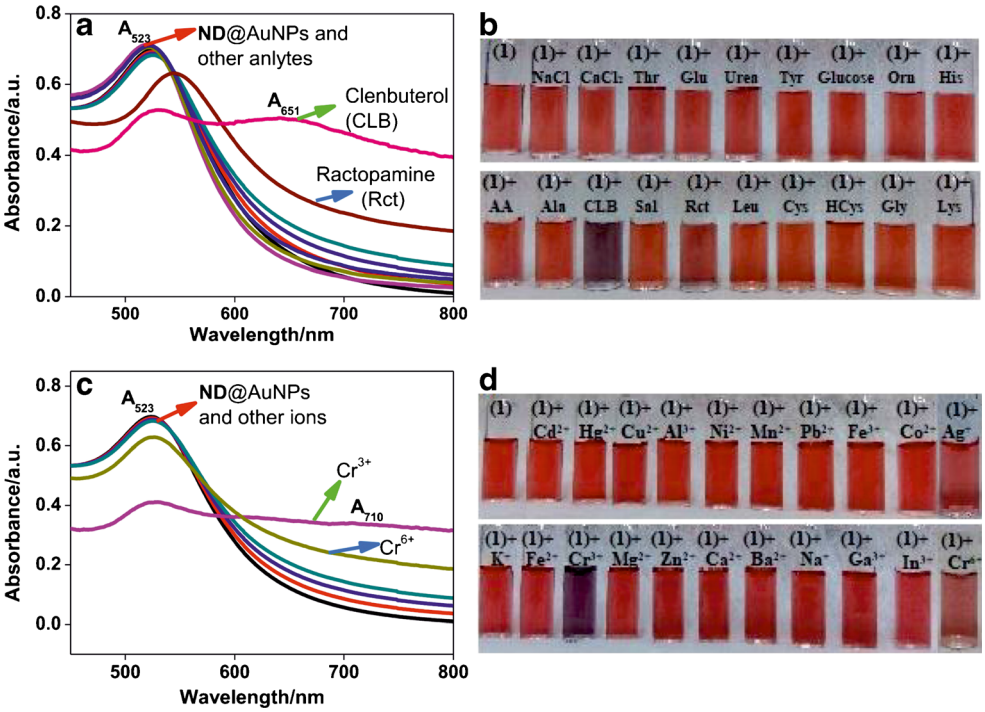

Fig. 2 **a, b** SPR changes of **ND**@AuNPs on selectivity towards CLB and Cr(III)at pH 6; **c, d** colorimetric responses of **ND**@AuNPs towards CLB and Cr(III)with other interferences at pH 6; Here, contrast to 3 μM of other interferences and 5 μM of Cr^{6+} ions, 1 μM of CLB and Cr(III)were used

observed through the complete disappearance of original broad band between 2900~3500 cm^{-1}. In addition, symmetrical amide –NH stretch is upshifted from 1412 to 1382 cm^{-1}.

Akin to CLB, **ND**@AuNPs with Cr(III) also displayed the differential FTIR spectra as envisioned in Fig. S31 (ESM). Where, the upshifted –C-N stretching bands are exhibited at 1160 and 2345 cm^{-1}. On the other hand, coordination of Cr(III) ions led to ultimate vanishing of amide -NH band with broadened and upshifted symmetrical stretch observed at 1394 cm^{-1}. Additionally, a broad low intense amide –C=O stretch is upshifted at 1632 cm^{-1}. These FTIR studies authenticated the contribution of amide –NH and –C=O groups towards

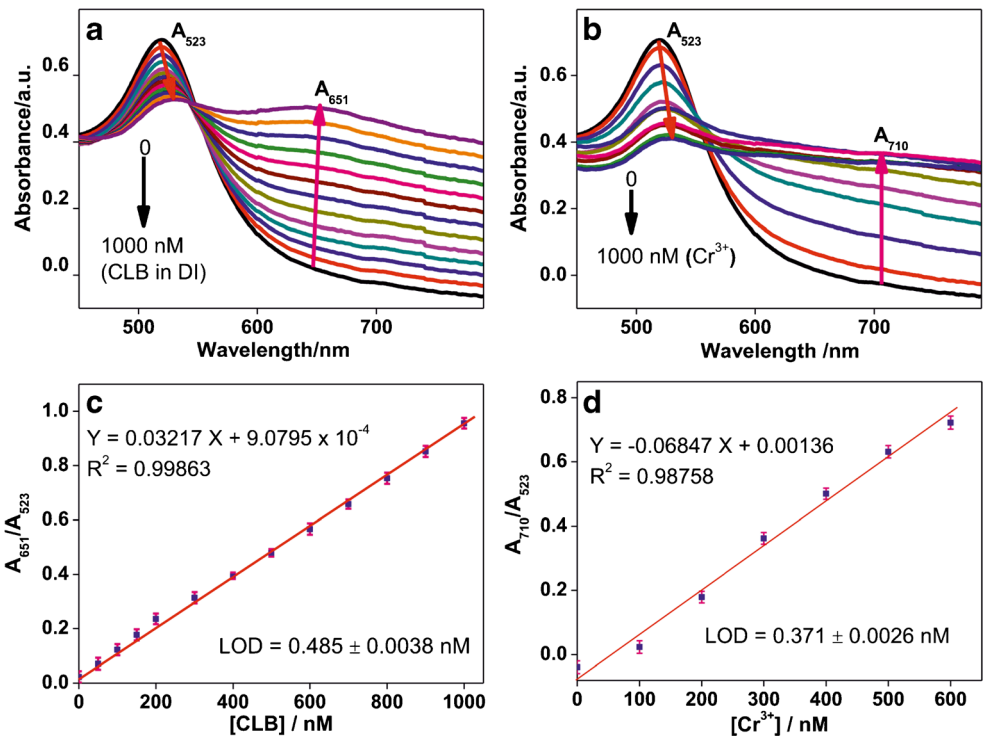

Fig. 3 UV-Vis titrations of **ND**@AuNPs with different concentrations of (**a**) CLB and (**b**) Cr(III)ions in DI water, at pH 6; Detection limits calculation on (**c**) CLB and (**d**) Cr(III)ions via standard deviation and linear fittings

Table 1 The recovery values of spiked Cr^{3+} ions in real samples

Sample	Spiked (μM)	Detected (μM) (mean[a] ± SD[b], $n = 3$)	Recovery (%)	RSD (%)	ICP-MS observed (μM)
tab water	0	ND[c]	–	–	ND[c]
	0.01	0.0098 ± 0.002	98.01	1.23	0.0101
	0.25	0.252 ± 0.004	101.02	1.66	0.263
	1	1.062 ± 0.025	106.23	2.31	1.087
Lake water	0	ND[c]	–	–	ND[c]
	0.01	0.0103 ± 0.006	103.03	0.67	0.011
	0.25	0.261 ± 0.024	104.54	1.15	0.268
	1	1.142 ± 0.012	114.16	1.83	1.166
Urine	0	ND[c]	–	–	ND[c]
	0.05	0.053 ± 0.005	106.02	1.12	0.0548
	0.25	0.261 ± 0.011	104.45	1.29	0.249
	1	1.122 ± 0.016	112.28	1.53	1.129

[a] mean of three measurements

[b] SD: standard deviation

[c] Not detected

CLB and Cr(III) ions detection via coordination or H-bonding induced aggregation and hence possible mechanisms are suggested in Figs. S32 and S33 (ESM). Wherein, ND act as functional groups carrier and enhance the disaggregation of AuNPs in the absence of analytes via steric effect. Moreover, those functional groups present in **ND**@AuNPs forms the complex with CLB or Cr(III) ions and then led to color changes through aggregation.

Afterward, from the individual titrations of CLB and Cr(III) ions (Fig. 3a, b), the linear ranges of CLB and Cr(III) recognition are established as $1.05 \times 10^{-8} \sim 0.98 \times 10^{-6}$ and $1.3 \times 10^{-8} \sim 1.04 \times 10^{-6}$, respectively. Similarly, according to the 3σ (signal-to-noise) standards [31] by using the linear regression equations of $y = 0.03217\times + 9.0795 \times 10^{-4}$ ($R^2 = 0.999$, $n = 3$) and $y = -0.06847\times + 0.00136$ ($R^2 = 0.988$, $n = 3$), the LODs of CLB and Cr(III) ions are estimated as 0.485 ± 0.0038 and 0.371 ±

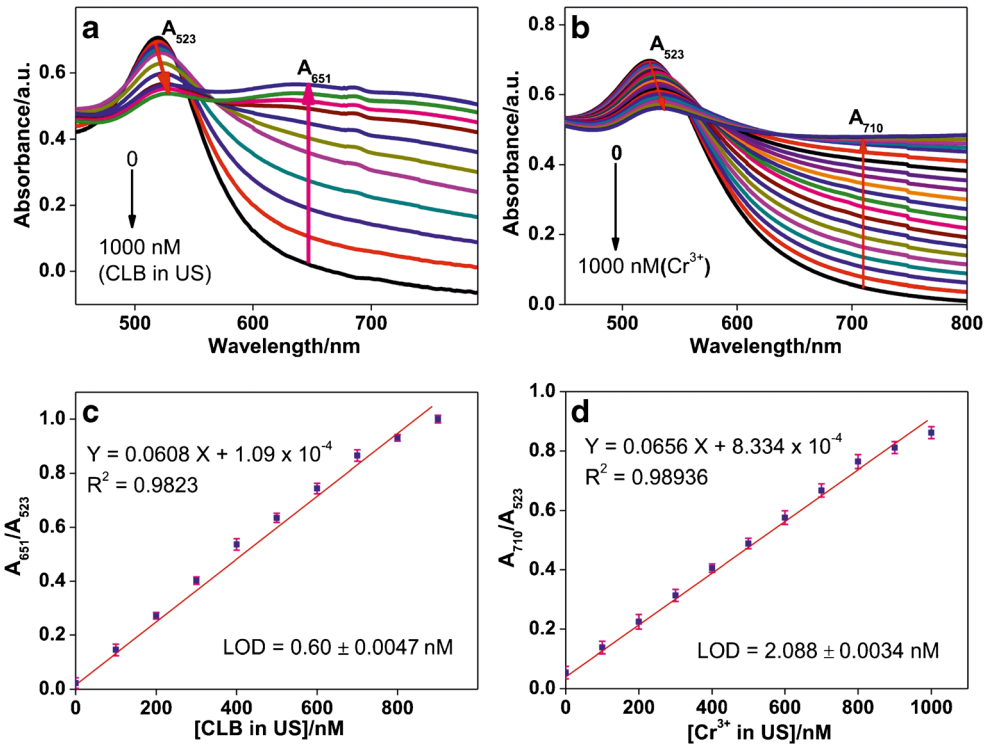

Fig. 4 UV-Vis titrations of **ND**@AuNPs with different concentrations of (**a**) CLB and (**b**) Cr(III)ions in human urine samples [US], at pH 6; Detection limits calculation on (**c**) CLB and (**d**) Cr(III)ions via standard deviation and linear fittings

Table 2 The recovery values of spiked CLB in DI water and urine samples

Sample	Spiked (μM)	Detected (μM) (mean[a] ± SD[b], n = 3)	Recovery (%)	RSD (%)
DI water	0	ND[c]	–	–
	1	0.99 ± 0.006	99.31	2.41
	2.5	2.486 ± 0.012	99.47	2.13
	5	5.112 ± 0.022	102.68	1.95
Urine	0	ND[c]	–	–
	1	1.053 ± 0.008	106.12	1.42
	2.5	2.497 ± 0.024	99.84	1.99
	5	4.911 ± 0.026	98.28	2.73

[a] mean of three measurements

[b] SD: standard deviation

[c] Not detected

0.0026 nM, correspondingly, as represented in Fig. 3c, d. It is important to note that the LODs of those analytes are much lower and hence can be applied in real time monitoring as revealed next.

Cr(III) detection in real water studies

In this examination, NCTU lake and tap water samples are exploited [18, 32]. Wherein, the ICP-MS based estimation was in agreement with the calibration curves of **ND**@AuNPs SPR shifts to those respective Cr(III) concentrations and evidenced a relative error of less than 2.5% as presented in Table 1. The recovery of Cr(III) in tap and lake water are fallen between 98.01~106.23 and 103.03~114.16%, consistently. Hence confirm the real time application of this method. In a similar fashion, the human urine samples based colorimetric assay [33] are accounted as follows.

Detection of CLB and Cr(III)in human urine sample

As seen in Figs. S34 and S35 (ESM), colorimetric changes of the probe are induced by CLB and Cr(III) from 400 nM onwards. Whereas, from the individual titrations (Fig. 4a, b), the linear ranges of CLB and Cr(III) detection in human urine samples are recognised as $1.9 \times 10^{-8} \sim 1.21 \times 10^{-6}$ and $2.7 \times 10^{-8} \sim 1.98 \times 10^{-6}$, respectively. From linear regression equations of $y = 0.0608\times + 1.09 \times 10^{-4}$ ($R^2 = 0.982$, $n = 3$) and $y = 0.0656\times + 8.334 \times 10^{-4}$ ($R^2 = 0.989$, $n = 3$), the LODs of CLB and Cr(III) in urine studies are calculated as 0.60 ± 0.0047 and 2.088 ± 0.0034 nM, individually, as exposed in Fig. 4c, d. Similarly, urine samples based assay of Cr(III) displays the better recovery (104.45~112.28%) with less than 2% relative error (RSD) as shown in Table 1. In the same way, the recovery of CLB in spiked DI water and urine samples are lies between 99.31~102.68% and 98.28~106.12%, correspondingly, with less than 3% RSD as seen in Table 2. Further to elaborate, as presented in Tables S2 and S3 (ESM), **ND**@AuNPs displayed the better performance in CLB and Cr(III) detection than that of previous reports.

Conclusion

A nanodiamond conjugated gold nanoparticles (**ND**@AuNPs) is firstly reported as an analytical probe for the selective assay of CLB and Cr(III) ions. Here, the consumed low toxic nanodiamond derivative (**ND-Thiol)** act as a functional group carrier, which may interact with analytes. But, the stability of **ND**@AuNPs are restricted to the 10 $ng.mL^{-1}$ concentration of **ND-Thiol**. The complexation between amide (–C=O and –N-H) functional groups of **ND**@AuNPs with CLB or Cr(III) ions are responsible for the aggregation induced color changes. Nevertheless, this assay seems to be more effective after 25 min and at pH 6. Further to notice, the real analysis on this assay protract its vision to biological applicability in future.

Acknowledgements The authors are grateful to the Ministry of Science and Technology of Taiwan for financially supporting this research under the contract MOST 105-2811-M-009-057 and MOST 105-2112-M-009-005-MY3.

Compliance with ethical standards The author(s) declare that they have no competing interests.

References

1. Soppa GKR, Lee J, Stagg MA, Felkin LE, Barton PJR, Siedlecka U, Youssef S, Yacoub MH, Terracciano CMN (2008) Role and possible mechanisms of clenbuterol in enhancing reverse remodelling during mechanical unloading in murine heart failure. Cardiovasc Res 77:695–706
2. Liu G, Chen H, Peng H, Song S, Gao J, Lu J, Ding M, Li L, Ren S, Zou Z, Fan C (2011) A carbon nanotube-based high-sensitivity electrochemical immunosensor for rapid and portable detection of clenbuterol. Biosens Bioelectron 28:308–313
3. Ventura R, Damasceno L, Farré M, Cardoso J, Segura J (2000) Analytical methodology for the detection of β_2-agonists in urine by gas chromatography–mass spectrometry for application in doping control. Anal Chim Acta 418:79–92
4. Xu T, Wang BM, Sheng W, Li QX, Shao XL, Li J (2007) Application of an enzyme-linked immunosorbent assay for the detection of clenbuterol residues in swine urine and feeds. J Environ Sci Health B 42:173–177
5. Thevis M, Schebalkin T, Thomas A, Schänzer W (2005) Quantification of Clenbuterol in human plasma and urine by liquid chromatography-tandem mass spectrometry. Chromatographia 62: 435–439
6. Chen Y, Wang W, Duan J, Chen H, Chen G (2005) Separation and determination of Clenbuterol, Cimaterol and salbutamol by capillary electrophoresis with Amperometric detection. Electroanalysis 17:706–712

7. Yan F, Zhang Y, Zhang S, Zhao J, Liu S, He L, Feng X, Zhang H, Zhang Z (2015) Carboxyl-modified graphene for use in an immunoassay for the illegal feed additive clenbuterol using surface plasmon resonance and electrochemical impedance spectroscopy. Microchim Acta 182:855–862
8. He P, Shen L, Liu R, Luo Z, Li Z (2011) Direct detection of β-agonists by use of gold nanoparticle-based colorimetric assays. Anal Chem 83:6988–6995
9. Vincent JB (2000) The biochemistry of chromium. J. Nutrition 130: 715–718
10. Li D, Li C-Y, Qi H-R, Tan K-Y, Li Y-F (2016) Rhodamine-based chemosensor for fluorescence determination of trivalent chromium ion in living cells. Sensors Actuators B Chem 223:705–712
11. Shrivastava R, Upreti RK, Seth PK, Chaturvedi UC (2002) Effects of chromium on the immune system. FEMS Immun Med Microbiol 34:1–7
12. Chang Y-L, Jiang S-J (2001) Determination of chromium in water and urine by reaction cell inductively coupled plasma mass spectrometry. J Anal At Spectrom 16:1434–1438
13. Rakhunde R, Deshpande L, Juneja HD (2012) Chemical speciation of chromium in water: a review. Critical rev. Environ Sci Technol 42:776–810
14. Gumpu MB, Sethuraman S, Krishnan UM, Rayappan JBB (2015) A review on detection of heavy metal ions in water – an electrochemical approach. Sensors Actuators B Chem 213:515–533
15. Hassan SSM, El-Shahawi MS, Othman AM, Mosaad MA (2005) A potentiometric rhodamine-B based membrane sensor for the selective determination of chromium ions in wastewater. Anal Sci 21: 673–678
16. Li M, Zhang D, Liu Y, Ding P, Ye Y, Zhao Y (2014) A novel colorimetric and off–on fluorescent Chemosensor for Cr^{3+} in aqueous solution and its application in live cell imaging. J Fluoresc 24: 119–127
17. J-X D, Li Y-H, Guan R (2007) Chemiluminescence determination of chromium(III) and total chromium in water samples using the periodate-lucigenin reaction. Microchim Acta 158:145–150
18. Shellaiah M, Simon T, Sun KW, Ko F-H (2016) Simple bare gold nanoparticles for rapid colorimetric detection of Cr3+ ions in aqueous medium with real sample applications. Sensors Actuators B Chem 226:44–51
19. Zhang Z, Duan F, He L, Peng D, Yan F, Wang M, Zhong W, Jia C (2016) Electrochemical clenbuterol immunosensor based on a gold electrode modified with zinc sulfide quantum dots and polyaniline. Microchim Acta 183:1089–1097
20. Khan A, Parwaz Khan AA, Rahman MM, Asiri AM, Alamry KA (2015) Preparation of polyaniline grafted graphene oxide-WO3 nanocomposite and its application as a chromium(iii) chemi-sensor. RSC Adv 5:105169–105178
21. Cheng L-C, Chen HM, Lai T-C, Chan Y-C, Liu R-S, Sung JC, Hsiao M, Chen C-H, Her L-J, Tsai DP (2013) Targeting polymeric fluorescent nanodiamond-gold/silver multi-functional nanoparticles as a light-transforming hyperthermia reagent for cancer cells. Nano 5:3931–3940
22. Shellaiah M, Chen TH, Simon T, Li L-C, Sun KW, Ko F-H (2017) An affordable wet chemical route to grow conducting hybrid graphite-diamond nanowires: demonstration by a single nanowire device. Sci Rep 7:11243
23. Németh P, Garvie LAJ, Buseck PR (2015) Twinning of cubic diamond explains reported nanodiamond polymorphs. Sci Rep 5: 18381
24. Zhang G, Jasinski JB, Howell JL, Patel D, Stephens DP, Gobin AM (2012) Tunability and stability of gold nanoparticles obtained from chloroauric acid and sodium thiosulfate reaction. Nanoscale Res Lett 7:337
25. Lü X, Song Y, Zhu A, Wu F, Song Y (2012) Synthesis of gold nanoparticles using Cefopernazone as a stabilizing reagent and its application. Int J Electrochem Sci 7:11236–11245
26. Tang H, Wang M, He D, Zou Q, Ke Y, Zhao Y (2016) Synthesis of nano-polycrystalline diamond in proximity to industrial conditions. Carbon 108:1–6
27. Techane SD, Gamble LJ, Castner DG (2011) X-ray photoelectron spectroscopy characterization of gold nanoparticles functionalized with amine-terminated alkanethiols. Biointerphases 6:98–104
28. Kang J, Zhang Y, Li X, Miao L, Wu A (2016) A rapid colorimetric sensor of clenbuterol based on cysteamine-modified gold nanoparticles. ACS Appl Mater Interfaces 8:1–5
29. Zhang X, Zhao H, Xue Y, Wu Z, Zhang Y, He Y, Li X, Yuan Z (2012) Colorimetric sensing of clenbuterol using gold nanoparticles in the presence of melamine. Biosens Bioelectron 34:112–117
30. Cui H, Wang W, Duan C-F, Dong Y-P, Guo J-Z (2007) Synthesis, characterization, and electrochemiluminescence of luminol-reduced gold nanoparticles and their application in a hydrogen peroxide sensor. Chem Eur J 13:6975–6984
31. Zhan L, Yang T, Zhen SJ, Huang CZ (2017) Cytosine triphosphate-capped silver nanoparticles as a platform for visual and colorimetric determination of mercury(II) and chromium(III). Microchim Acta 184:3171–3178
32. Lee IL, Sung Y-M, C-H W, S-P W (2014) Colorimetric sensing of iodide based on triazole-acetamide functionalized gold nanoparticles. Microchim Acta 181:573–579
33. Du J, Zhu B, Chen X (2013) Urine for plasmonic nanoparticle-based colorimetric detection of mercury ion. Small 9:4104–4111